Makara Journal of Technology

Volume 21 | Issue 2 Article 1

8-2-2017

Residual Stress Measurements on the TIG Weld Joint of 57Fe15Cr25Ni Austenitic Steel for Structural Material Applications by Means X-Ray Diffraction Techniques

Parikin Parikin
Center for Science and Technology of Advanced Materials, National Nuclear Energy Agency (BATAN), Puspiptek Serpong, South Tangerang 15314, Indonesia, farihin@batan.go.id

Agus Hadi Ismoyo
Center for Science and Technology of Advanced Materials, National Nuclear Energy Agency (BATAN), Puspiptek Serpong, South Tangerang 15314, Indonesia

Riza Iskandar
Central Facility for Electron Microscopy (GFE), RWTH Aachen University, Ahorn Strausse 55, D-52074 Aachen, Germany

Arbi Dimyati
Center for Science and Technology of Advanced Materials, National Nuclear Energy Agency (BATAN), Puspiptek Serpong, South Tangerang 15314, Indonesia

Recommended Citation

Parikin, Parikin; Ismoyo, Agus Hadi; Iskandar, Riza; and Dimyati, Arbi (2017) "Residual Stress Measurements on the TIG Weld Joint of 57Fe15Cr25Ni Austenitic Steel for Structural Material Applications by Means X-Ray Diffraction Techniques," *Makara Journal of Technology*: Vol. 21: Iss. 2, Article 1.
DOI: 10.7454/mst.v21i2.3080
Available at: https://scholarhub.ui.ac.id/mjt/vol21/iss2/1

Makara J. Technol. 21/2 (2017), 49-57
doi: 10.7454/mst.v21i2.3080

Residual Stress Measurements on the TIG Weld Joint of 57Fe15Cr25Ni Austenitic Steel for Structural Material Applications by Means X-Ray Diffraction Techniques

Parikin[1*], Agus Hadi Ismoyo[1], Riza Iskandar[2], and Arbi Dimyati[1]

1. Center for Science and Technology of Advanced Materials, National Nuclear Energy Agency (BATAN), Puspiptek Serpong, South Tangerang 15314, Indonesia
2. Central Facility for Electron Microscopy (GFE), RWTH Aachen University, Ahorn Strausse 55, D-52074 Aachen, Germany

[*]*e-mail: farihin@batan.go.id*

Abstract

Measurements of residual stress on the 57Fe25Cr15Ni steel plate with no-filler TIG-welding process were carried out. This work was conducted to determine the nature of weld ability in synthesized steel. The bulks were formed in a dimension of 30x20x7 mm^3 to ease data retrieval. Results show that the largest residual stress occurred in the weld metal area, amounting to 82.40 MPa with lattice stretching of 0.18%. Conversely, the values decreased to 65.92 MPa and a stretch of 0.14% in the HAZ area. This residual stress is a tensile stress that can reduce the mechanical strength of the material since it adds to the applied loads. This was confirmed by microstructure observations. The carbon content was very high in the dark lines. Weaken materials usually start from this side and could initiate the intergranular cracks that rapidly migrate among its grain boundaries.

Abstrak

Pengukuran Tegangan Sisa pada Sambungan Las-TIG Bahan Struktur Baja Austenitik 57Fe15Cr25Ni Menggunakan Teknik Difraksi Sinar-X. Pengukuran tegangan sisa pada pelat baja 57Fe15Cr25Ni akibat proses pengelasan TIG tanpa filler telah dilakukan. Pekerjaan ini dilakukan untuk mengetahui sifat mampu las dari bahan pelat baja. Bahan 'bulk' dibentuk plat dengan dimensi 30x20x7 mm3 untuk memudahkan pengambilan data. Hasil penelitian menunjukkan bahwa tegangan sisa terbesar terjadi di daerah pusat las, sekitar 82,40 MPa dengan kisi peregangan 0,18% dan turun pada sekitar 65,92 MPa dengan regangan sebesar 0,14% di daerah HAZ. Tegangan sisa ini adalah tegangan tarik yang dapat mengurangi kekuatan mekanik material karena mampu menambah beban terpakai. Hal ini ditegaskan dengan pengamatan mikrostruktur. Kandungan karbon sangat tinggi di garis hitam. Pelemahan bahan biasanya dimulai dari sisi ini dan bisa mengawali retakan intergranular, yang dengan cepat dapat bermigrasi di antara batas butirnya.

Keywords: 57Fe25Cr15Ni alloy, no-filler welding, X-ray diffraction, scanning electron microscopy, optical microscopy

1. Introduction

In consideration of special material requirements for reactor structural constructions, steel needs to have special advantages for high temperature operations. This encourages independent material engineers in BATAN to synthesize material with significant local content. Previously, the laboratory scale of fabrications has been carried out using the methods of casting [1], by making a series of austenitic (A) and ferritic (F) superalloy steels. The A&F series of steel are of non-standard composition and low-carbon steel, which is a mixture of local components. Until now, two series of Austenitic (A1 & A2) and Ferritic (F1 and F2) steels have been made. When good steel has been characterized, it is expected to be applied as a candidate material structure of a nuclear reactor in particular (construction) zone.

As a standard safety criteria requirement for reactor, structural materials which, among others, are the water-cooled reactor, particularly vessel and heat exchanger – must cover the following requirements: withstanding the mechanical loads, corrosion resistant, high-temperature resistant, and resistant to neutron irradiation [2]. The purpose of synthesizing the austenitic super alloy is to create a new austenitic type of materials with higher

nickel content, having reduced the titanium content or no titanium at all. That way, the mechanical properties of the materials should be significantly improved.

The engineering properties of materials and structural components notably fatigue life, distortion (welding), dimensional stability (rolling), corrosion resistance, and brittle fracture can be considerably influenced by residual stresses [3]. Such effects usually cause considerable expenditure in repairs and restoration of parts, equipment, and structures.

Accordingly, residual stresses analysis is a compulsory stage in the design of parts and structural elements and in the estimation of their reliability under real service conditions. Systematic studies have shown that, for instance, welding residual stresses might lead to a drastic reduction in the fatigue strength of welded elements. In multi-cycle fatigue (N > 106 cycles), the effect of residual stresses is comparable to the effect of stress concentration [4]. Surprisingly, the effect of residual stresses on the fatigue life of welded elements, specifically with regards to relieving harmful tensile residual stresses and introducing beneficial compressive residual stresses in the weld toe zones, is significant.

One of the areas for consideration among the welds is the heat affected zone (HAZ), which is the area directly affected by the heat treatment of the weld. Failure of the construction component generally stems from connection between the components, especially in the HAZ. In this area, the material experiences changes in the microstructures and mechanical properties, which can be fatal if neglected. Continuous research needs to be done to know the influences of the welding process, especially in materials for specific purposes, such as structural materials for nuclear power plants.

Many techniques exist for the measurement of residual stresses within engineering components; however, it is the effects of the residual stresses that are actually measured, not the stresses themselves. Recently, welding effects around the weld-joint have been inspected to obtain information regarding stress behaviors in three regions, i.e. weld metal, heat-affected zone, and base metal, by means of X-ray diffraction technique. These regions near the weld line undergo severe thermal cycles due to the intense concentration of heat in the heat source of welding. Thermal cycles cause non-uniform heating and cooling in the material, thus generating inhomogeneous plastic deformation and residual stresses in the weld metal. The presence of residual stresses can be detrimental to the performance of the welded product. Tensile residual stresses are generally detrimental, since they increase the susceptibility of a weld to fatigue damage, stress corrosion cracking and fracture.

Furthermore, a residual stress may be created during the manufacturing process of a material, or it may accumulate in a structure over many years in operation. In either case, such a stress can adversely affect a product's quality, durability, and lifetime. Therefore, an accurate detection of residual stress is an important element of the quality control process. It also helps predict the service lifetime of products. Residual stresses, both on exceptionally strained points and on the surfaces of moving parts, are routinely determined by an X-ray diffraction (XRD) [5]. XRD is presently used to measure residual stress non-destructively. In addition, XRD allows non-contact measurements with the unsurpassed spatial resolution and the ability to measure hardened materials. One way to perform residual stress measurements is by obtaining the whole pattern of diffraction data, which is usually accompanied using software implementing the Rietveld refinement method, simply known as the Rietveld method. The Rietveld method is capable of handling diffraction data obtained from X-ray diffractometers. Theoretical prediction of residual stresses using diffraction techniques has been explained in literature [5].

The aim of this research is to investigate the presence of residual stresses in 57Fe25Cr15Ni alloy, which is utilized as a reactor structure material after welding process has been applied, by means of tailoring X-ray diffraction and Rietveld refinement method [6]. Our observation was concentrated in three main regions, i.e. the weld metal, the heat-affected zone (HAZ), and the base metal.

2. Experimental

The primary raw materials employed in the fabrication of the austenite stainless steel alloy are granular ferro scrap, nickel, ferro-chrome, ferro-manganese, ferro-silicon, etc. These minerals have been extracted from domestic mines, thus creating an economic advantage because there is no need to purchase expensive imports, since much cheaper alternatives are available domestically. The elemental compositions of product materials are listed in Table 1, as obtained with a 1996 Swiss-made Optical Emission Spectrometry (OES) in Bandung Manufacture Polytechnique.

Table 1. Type and Chemical Composition of the Specimen

Specimen	Reduction (%)	Remarks
A2-type	70	TIG-Weld no filter
57Fe15Cr25Ni Steel		Dimension: 30 x 20 x 7 mm^3
		Hardness= 126.86 kgf/mm^2

Elemental Composition (%wt.)										
Fe	**Cr**	**Ni**	**Mn**	**Si**	**C**	**Ti**	**S**	**P**	**Cu**	**Nb**
87.74	15.42	25.01	0.32	0.96	0.34	Inpurity <0.1				

The fractional quantities of each constituent component from the base materials are computed, then an appropriate amount of these base materials is weighed separately on the micro scale. Meanwhile, a mould made of silica-sand is simultaneously constructed by mixing a bentonite binder with a little water. The finished mould must now be lined up with a certain choice of material, depending on the appropriate acid-, base- or neutral environment. A neutral type lining is a standard requirement if the desired product is stainless alloy. As a final step, the lining wall is now sintered. Production of stainless steels requires a neutral environ- ment, and this calls for an alumina (Al_2O_3) lining material used with a specific type of ramming binder.

The microstructure characterization is accomplished using an optical microscope and a Scanning Electron Microscope [7]. The crystalline space group is verified by collecting reflection intensities using an X-ray diffractometer. Meanwhile, density measurement is carried out using a sigmat and microbalance, and the hardness testing is carried out using the Vickers indentation method. Optical Emission Spectrometry (OES) equipment is employed in the elemental composition measurement, and the sample is specially prepared by a spark erosion method to have a dimension of 2.5 x 2.5 x 12 cm^3.

Figure 1 shows the macrostructures of the specimen used in this work. Test material is in the form of base metal austenitic steel A2 type with a dimension of 30x20x7 mm^3. The specimen is initially hot-rolled and cut into two pieces, and then given TIG welding (tungsten inert gas) without filer with a current 60 mA. Figure 1 a- c shows the specimens of base metal and weld cross section in longitudinal and transverse sides. Certified welding process was performed by professionals at the Center for Engineering and Nuclear Facilities (PRFN) - BATAN Serpong. The laboratory preparation was then followed by grinding and polishing processes and smoothing surface with 180-2500 mesh grid paper, so that the effect of surface roughness when diffracted can be minimized.

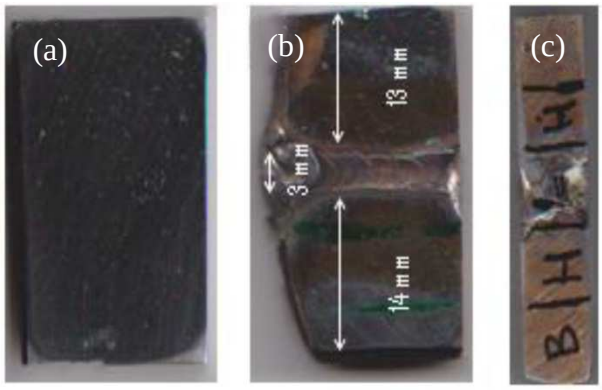

Figure 1. Macrostructures of Unpolished Specimen: (a) Base Metal, (b)-(c) TIG-weld Longitudinal and Transversal, Respectively

The welding process was carried out without filler using GTAW (Gas Tungsten Arc Welding) method, commonly known as the TIG welding. Before the welding process, the specimen was prepared with the following stages. First, an initial cleansing was conducted with a strong spray of air, so that the tip of the specimen to be welded was free from impurities. Next, the welding specimens were prepared on the flat side (as accepted) as shown in the schematic Figure 2. With the melting method, the ends of the metal were glued together in the scope of argon gas atmosphere, and the movement of the welding speed was controlled. Parameters used in the welding process are shown in Table 2.

The measurement of X-ray diffraction patterns with the Cu target was conducted at the Center for Science and Technology of Advanced Materials (PSTBM) - BATAN, using the step-counting mode between the angle of 2θ = 40° and 100°, and preset time of 2 seconds. The X-ray beam shoot was directed at three main regions, namely the welding center/weld metal (WM), the heat affected zone (HAZ), and the Base Metal (BM). The process of area separations or sectioning for precision of the shooting zone files in the X-ray diffraction measurements was performed by using double tapes and plastic tapes as covers, in order to obtain real data according to their respective regions. The diffraction pattern blank samples (double tapes and plastic tapes) were also taken as a correction to the data acquisition on each diffraction pattern in a particular area. Further data analysis was performed by using the diffraction pattern of RietAn'94 software, to obtain the refined crystallographic parameters with high reliability factors and satisfactory goodness of fit.

Table 2. Parameters of the Welding

TIG-Weld Parameter	
Welding type	GTAW
Dimension	30 x 20 x 7 mm
Atmosphere	Argon
Currents	60 A
Voltage	50 V
Speed	120 mm/min

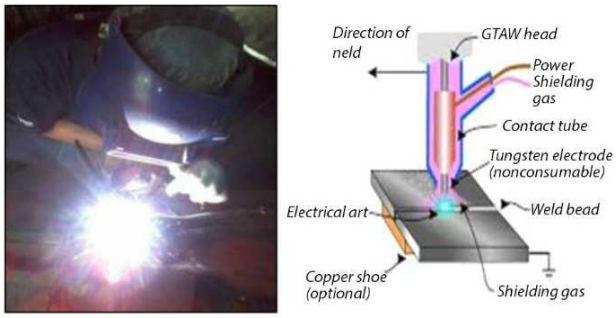

Figure 2. Scheme and TIG (Tungsten Inert Gas) Welding Process without Filler

3. Results and Discussion

X-ray Diffraction Profiles. Figure 3 shows the X-ray diffraction patterns of three measurable areas, namely the base metal, the HAZ, and the weld metal, using a wavelength of about 1.54 Å. The entire diffraction pattern shows five dominant diffraction peaks, which is typical for a face-centered cubic crystal system (*fcc*). Peaks appearing at successive diffractogram are the (111), (200), (220), (311) and (222) planes. These fields are numerically grouped according to odd or even numbers, diffracted at the consecutive 2θ-angle of 43.50°, 50.60°, 74.60°, 90.65°, and 95.90°. However, the diffraction patterns that are contaminated by the odd minor peaks could enhance the background counts. These scattered specimens are from the amorphous materials, such as cellophane tape (plastic tape) as the closing/separator firing zone file, while measurements were taken (see the inserted scheme in Figure 4). This pattern is reinforced in the identification of the results of scanning/enumeration blank sample diffractogram shown in Figure 4. The contamination of these diffraction peaks are in the range of measurement angles between 43°-43.10°; 46°-49° and 53°-66°. The peaks are very undesirable

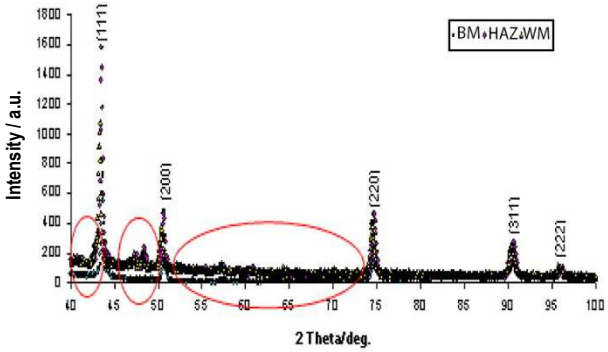

Figure 3. X-ray Diffraction Profiles of Specimens in TIG-Welding without a Filler in the Area: Base Metal, Heat Affected Zone, and Weld Metal

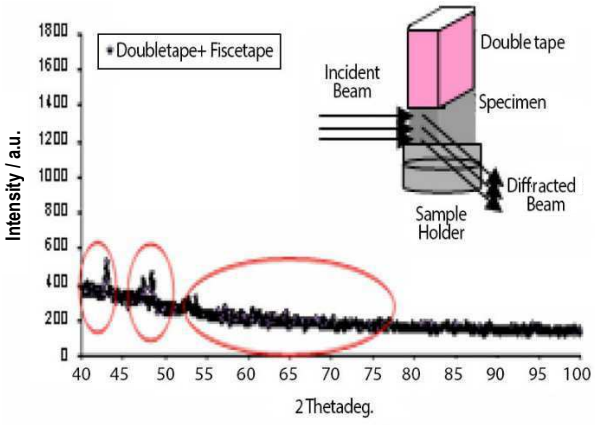

Figure 4. X-ray Diffraction Profile of Blank Specimens (double tape + plastic tape) and Inserted Scheme

contaminants and can hinder the process of fitting the data because it is very difficult to achieve the convergence of the iteration calculation nice. Diffractogram in Figure 4 is the data correction to the acquisition of the diffraction pattern of each zone on the diffraction pattern of base metal, HAZ, and weld metal. Except for the diffraction pattern of base metal 2θ low-angle range, the effect of masking the peak contaminants do not occur because of the displacement of the specimen surface and tape. In the calculation of Rietan '94 program, the range of the diffraction angle was not taken into consideration to obtain an optimal reference number value of goodness of fit (R_{wp};S).

Rietveld Refinements. Table 3 informs the type of test specimen, i.e. the reduction and crystallographic data input in the process of calculating the Rietveld method. Data analysis was performed with software RietAn [5-6] and computed by MAUD program [8]. The program can compute the powder diffraction data obtained by X-ray and neutron. This program takes the initial crystallographic data as forming the pattern of the model and scans X-ray scattering chopped test specimens as forming the standard pattern. In Rietveld, the least square refinement (least squares) is performed until convergence is achieved (best fitting) between all observed diffraction patterns and entire patterns of the intensity calculation. This calculation is based on the simultaneous smoothing models and other characteristics, such as the lattice parameters, the effect of optical diffraction, and the factor modeling the desired appropriate instrument. The key to the solution is the feedback for smoothing between the working knowledge of the structure and the allocation of the Bragg reflection intensity observations of individual mutually overlapping portions.

Figure 5 displays the pattern for a Rietveld refinement of the weld metal measurement zone, HAZ, and the base metal, after the process of contaminant plastic tapes are excluded from the data. In the picture, there is one sign of line broadening, i.e. a line under standard patterns and models. This line indicates the position of the austenite phase in the steel specimens 57Fe15Cr25Ni. The full pattern of standard profiles and smoothing are successively displayed in the picture. The refinements clearly show the structure of a face-centered cubic crystal system, from

Table 3. Initial Parameters for Rietveld Refinements

Specimen	Reduction (%)	Remarks
A2-type 57Fe15Cr 25 Ni Steel (70A2)	70	Index Table: 1-225; Crystal Structure: FCC; Space Group: Fm3m; Lattice Parameters: A=b=c=3.56996 Å $\alpha = \beta = \gamma = 90°$

the figures reflecting plane (111), (200), (220), (311), and (222), which are patterned as all even or all odd. There is no evidence of any other phase in all the diffraction patterns obtained in each zone. Specimens treated with the TIG welding without filler can be assumed for the entire zone as a measure of the total face-centered cubic (*fcc*). The refinement was performed using single-phase models, namely the austenite phase (γFe) with space group Fm3m (I-225). The predicted initial lattice parameters of the carbon content (C) in the steel specimens were conducted using the relation a (Å) = 3.555 + 0.044x for austenite structure, with x as the weight percent of carbon [5]. The lattice parameters for steel 57Fe15Cr25Ni with the carbon element content of 0.34% by weight is 3.56996 Å, which is used as an early input into the calculation process RietAn'94.

The crystallographic parameters of the Rietveldrefinement results are compiled in Table 4. The profile shape of the peak phases were separately modeled using the pseudo-Voight function, which is a linear combination between Gaussian and Lorentzian functions. For the data acquisition angular of these experiments to be reliable, a parameter phase structure may be refined. These data include lattice parameter, isotropic thermal parameters, deviation of the zero point, anisotropic parameter (preferred orientation), and the profile parameters. Smoothing phase models are quite satisfactory, with R_{wp} that varies between 14% and 20% with a reliability factor S of 1.3 (listed in Table 4). This value still has a quite high statistical probability because it obstructs the process of fitting the data to peak (111) that is significantly contaminated by a peak blank sample/masking tape around the corner of 2θ = 43° (see Figure 5), making it very difficult to achieve convergence. The smoothing parameter lattice and peak profiles for the austenite phase slightly shifted from the zone to the measurement zones. Meanwhile, reliable thermal parameters were obtained from refining, and they are positively precious. Nevertheless, the diffraction pattern of the steel material is contributed by the effects of X-ray fluorescence (Kβ-line) of the element iron (Fe), which looks at the data elevated background. However, the peak to the background ratio is adequate and still distinguishable between the real diffraction peak and the chopped background.

Table 4. Parameter Results from Refinements

Zone	Lattice Parameters (Å)	U-fwhm (°)	Shified $2\theta_{311}$ (°)	GOF*	
				Rwp	*S*
WM	3.59710(54)	0.021946898	90.51	14.15	1.38
HAZ	3.59579(54)	0.05443586	90.55	17.72	1.74
Base Metal	3.59055(33)	0.02843829	90.72	20.43	1.31

* Goodness of fits

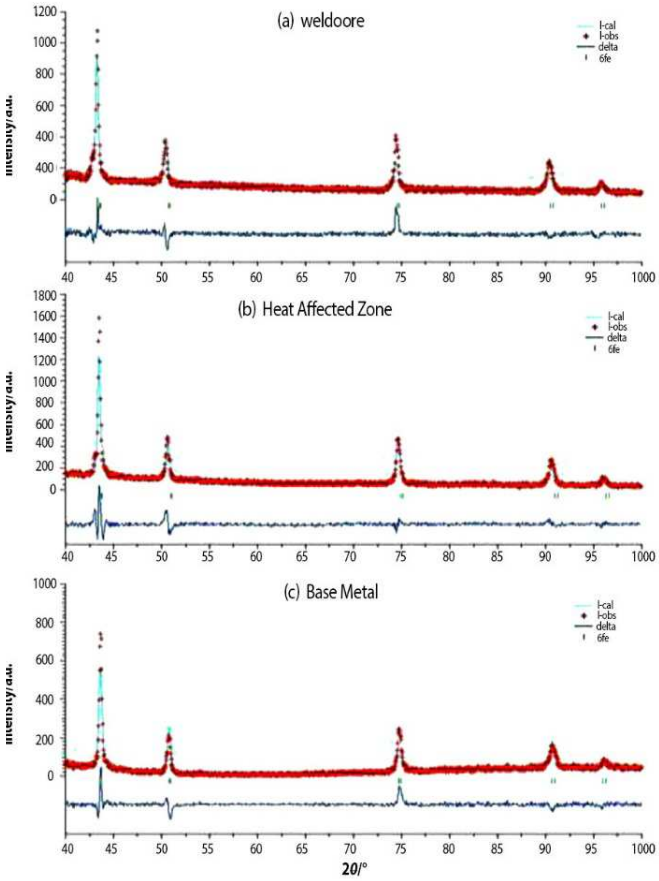

Figure 5. Rietveld Refinement Pattern of X-ray Diffraction Results; (a) Weld Metal, (b) Heat Affected Zone (HAZ), and (c) Base Metal

Lattice Strains. Figure 6 shows a small shift at an angle 2θ to the field of reflection (311) diffraction pattern as measurement results of specimens of steel 57Fe15 Cr25Ni. Changes occur due to the influence of instantaneous TIG welding heat (thermal shock) in the process of joining two pieces of steel specimens. Shifting the reflection plane (311), we successively scanned each zone of base metal (BM) at an angle of diffraction 2θ = 90.72°, and towards the HAZ area and weld metal (WM) at an angle of diffraction 2θ = 90.55° and 90.43°. This shift towards the corner 2θ is an unidentified minor, or to the left so it is negative. With reference to the acquisition of the diffraction pattern of the field (311) for the base metal zone, a large shift or difference angle (Δ2θ) for consecutive two other zones are: 0.17° and 0.29°. This peak shift moves towards the left or towards the dhkl great value. The difference of 2θ can indicate the occurrence of stretch in the crystal lattice of the magnitude formulated with $\Delta 2\theta = -2\ \varepsilon \tan\theta$ [9]. The maximum intensity of the chopped peaks increased successively from the BM zone, WM, and HAZ of 739, 1077, 1582 counts. It is the consequence of the values of

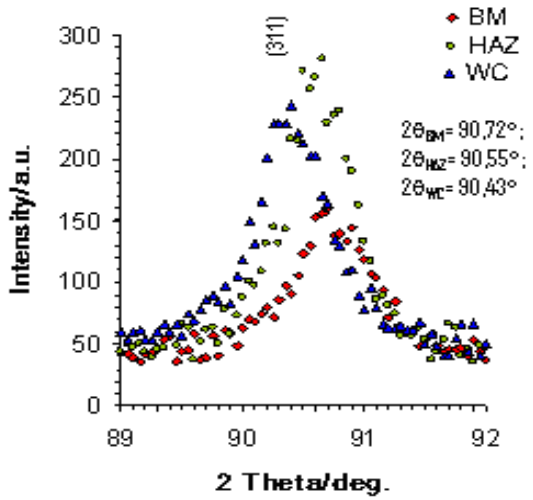

Figure 6. The Shift Angle X-ray Diffraction Around Welding Steel 57Fe15Cr25Ni Field of Reflection (311)

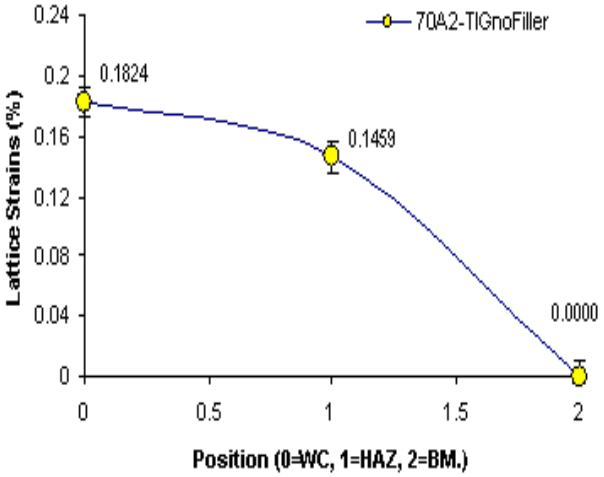

Figure 7. Stretching Around the Crystal Lattice Steel Welding 57Fe15Cr25Ni

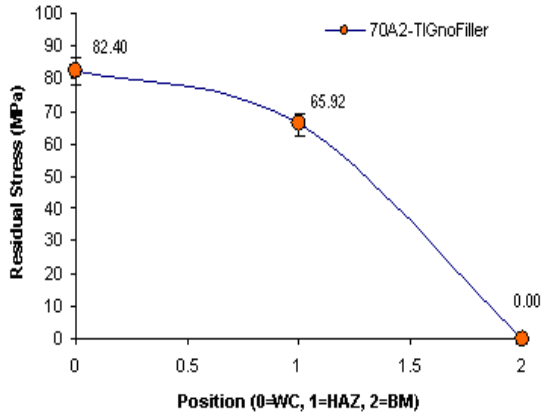

Figure 8. Hydrostatic Residual Stress Around Welding Steel 57Fe15Cr25Ni

full-width half maximum (fwhm) change. Peak broadening can be ascribed to the small particle size or the strain field homogenously or in both. The widening due to a small particle size appears in the form of Lorentzian functions, while the widening due to the strain is described by a Gaussian function. For example, the austenite phase peak broadening of the field of reflection (311) of the specimen TIG welding without a filler, which is shown in Figure 6. Strain field (e_{hkl}) in weld specimen tends to follow the normal function (gauss distribution). The Gaussian fitting of this peak is very convincing. Specimens of steel 57Fe15Cr25Ni that were observed in this experiment show some degrees of peak broadening. This widening of the diffraction profile indicates the existence of the strain field inhomogeneity. The width of half-fitting successive peaks in the region BM, HAZ, and WM amounted to 0.49°, 0.52°, and 0.47°, indicating that the strain field varies with the measurement zone of the weld specimen. The formulation of the strain field follows the equation: $U = U_O\text{-}32\ e^2_{hkl}\ \ln 2$ [5,10]. The actual value of the strain field is neither negative nor always positive. This field informs the strength of a field point hkl to stretch or expand.

Figure 7 shows the behavior of the average lattice strain in the specimen due to TIG welding. When the material is given a 70% reduction, the strain energy in the BM was approximately 0.25%, and got an extra hot welding of 0.18% in the WM and 0.15% in the HAZ. The increasing stretch crystal lattice is due to the absence of grain refinement by heat welding mechanism, which slightly increases the hardness of materials of approximately 115 HVN in the WM to 150 HVN in the HAZ. The average lattice strain mentioned above was obtained from a diffraction pattern for a wide angular region, which represents some average stretch in many directions in the field of diffraction. This method is the measurement of residual stress (hydrostatic), which complements the residual stress measurement along with the orientation.

Residual Stresses. Hydrostatic tension σ is directly proportional to the average strain in the formulation; $\sigma = [E/(1\text{-}2\nu)]\varepsilon_{av}$, where E is the Young's modulus and the Poisson comparator ν is determined from the measurements of its own. The regression parameters for sequential succession steel material are 187 GPa and 0.293 [10]. Figure 8 is a graph of residual stresses around the TIG-weld without a filler. For the case of single-phase austenitic structural steel (fcc), with values $\varepsilon_{av} = \varepsilon_a$, the tendency of the distribution of residual stresses from structural material of austenitic results of rolling is the tensile stress. Rolling up reduction 70%generates residual tensile stress of 9.7 MPa [10], while the residual stress due to welding heat adds to the existing stress of

82.40 MPa and 65.92 MPa in the WM and HAZ areas respectively. The behavior of residual stress [11] of this material follows the behavior of the crystal lattice strain (strain energy) on average, as seen in Figure 7.

Microstructures. Figure 9 shows SEM and OM images of the microstructures of the specimen around the weld joint. Three main areas can be observed, namely base metal (BM), heat affected zone (HAZ), and weld metal (WM). One of the interception areas is the thermo-mechanically affected zone (TMAZ). However, its boundary is not clear enough. This area is quite narrow and tends to be similar to the base metal due to its microstructures. In base metal, the microstructure exhibits elongated grains caused by the rolling process [12] during plate fabrication. Transversal deformation bands look narrow and elongated due to the hot rolling. Relatively large grains are observed to be approximately 3 μm, as measured in literature [9]. In HAZ, from the spherical grain formations, the effect of heat is obvious. The grains have changed from elongated to globular shapes, as visible nearby the center of the weld. The grain boundaries look like a dark line migrating to the weld metal. The carbon content might be very high in the dark lines. Weaken materials usually start from this side due to the presence of residual stress. This might initiate inter-granular cracks, which were able to migrate either slowly or rapidly among the grain boundaries.

An interesting phenomenon is visible in the center of the weld [13]. There are two overlapped phases in the form of cast structure (dendrites columnar) mixed with austenitic structure. The observation results of the center of the weld metal, in fact, are dominated by cast structure. However, at the same time, austenitic grains are very clearly formed in the background. Probably, a very rapid decrease from melting temperature to room temperature and the absence of filler in the welding process cause the cast structure to go back to the original form, i.e. its parent structure of the austenite phase. On the other hand, it is clearly seen that porosities are widely spread in the entire area of the weld metal. It looks like dark spots. It is assumed that this is due to the solid solution cooling process of the molten metal, which is very fast. It makes many air bubbles trapped in almost the entire surface of the weld metal. These may highly improve the value of residual stress in weld metal.

EDS spectrum. Processing the SEM image capture was carried out by using a secondary electron detector (SEI) on the acceleration energy of the primary electron beam source tungsten wire, by a maximum of 20 keV with a best condition. EDS was taken on the value of dead time on average between 20% and 40%. The EDS spectrum of the specimen taken around the weld joint is shown in Figure 10. The spectrums perform the spot area of (a) weld

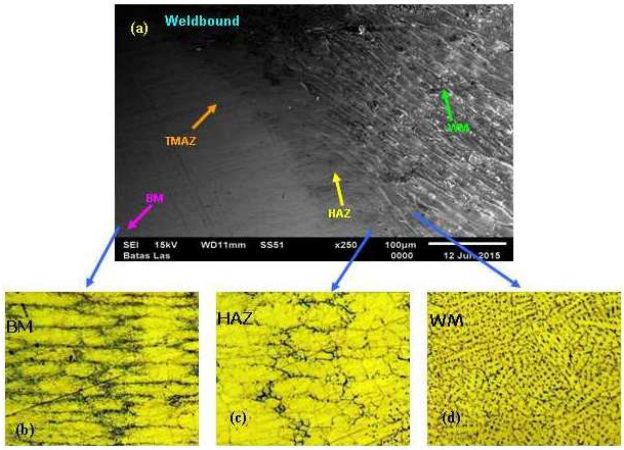

Figure 9. Scanning Electron Microscope (SEM-250x) and Light Optical Microscope (OM-10x) Images of the TIG Welded Specimen without a Filler: (a) Weldbound Over View, (b) Base Metal, (c) Heat Affected Zone, and (d) Weld Metal

metal and (b) heat affected zone and base metal. The percentage of the mass carbon contents slightly increased from 2.45% in HAZ to 2.73% in weld metal. This conforms to the microstructures shown in Figure 9c, where carbon elements migrate from HAZ to weld metal via grain boundaries. The Fe-Cr-Ni elements tend to have a constant mass fraction. However, there is an interesting phenomenon where Si and F elements emerge from the base metal area. The additional fraction of Si elements may be coagulated from the migrated Si into a certain enrichment place while other places are poor of Si elements. The presence of F elements may come from fluoride acid (HF) as the etching process was conducted in the preparations.

A comparative work with another residual stress measurement in the welding materials was conducted. It is shown that the curve behavior in Figure 8 of this research is the opposite to the other measurements in low carbon steel [14] weld pads on the root side of welding specimen after different weld passes as reported by Murugan, *et al*. [15]. Figure 11 shows the comparison of the residual stress data within both welding specimens, i.e. low carbon steel weld pads and weld-austenite superalloy steel (without using any filler). The residual stresses in former welding specimens tend to be in compression and to sharply increase in magnitude, whereas the last welding specimens are in tensile and steadily go down from base metal to weld metal position. In fact, the failures in welding materials with filler usually happen in the area between base metal and heat affected zone, while the no-filler welding materials are in the weld metal area. A similar study was explained in [16] to provide an accurate interpretation of the fatigue crack growth data on specimens extracted from

(a)

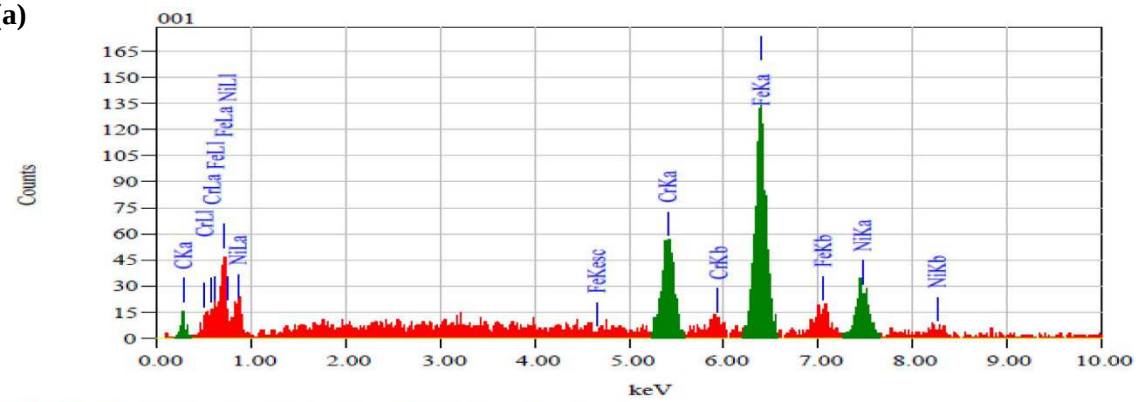

ZAF Method Standardless Quantitative Analysis
Fitting Coefficient : 0.3317

Element	(keV)	Mass%	Error%	Atom%	Compound	Mass%	Cation	K
C K	0.277	2.73	0.03	11.56				0.7799
Cr K	5.411	14.71	0.18	14.37				16.3489
Fe K	6.398	59.66	0.27	54.26				60.6364
Ni K	7.471	22.90	0.50	19.81				22.2348
Total		100.00		100.00				

(b)

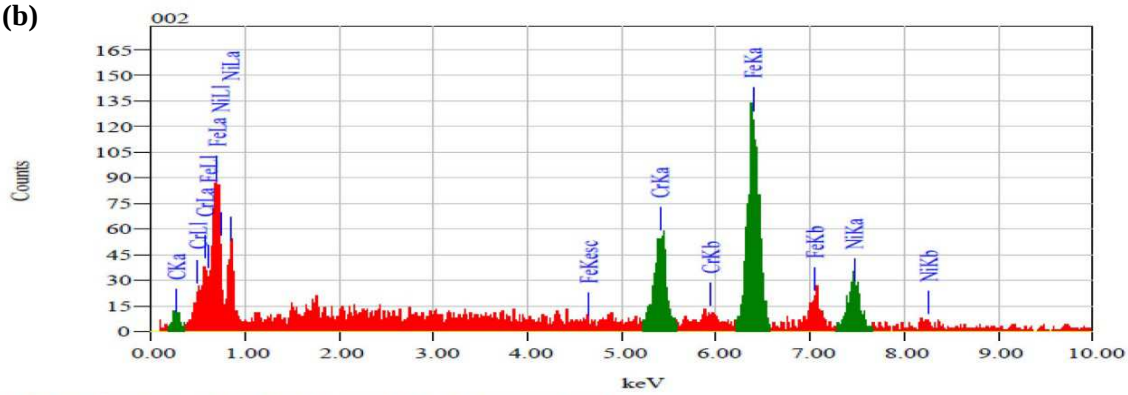

ZAF Method Standardless Quantitative Analysis
Fitting Coefficient : 0.3340

Element	(keV)	Mass%	Error%	Atom%	Compound	Mass%	Cation	K
C K	0.277	2.45	0.04	10.46				0.6939
Cr K	5.411	14.68	0.21	14.49				16.2561
Fe K	6.398	58.55	0.32	53.79				59.4582
Ni K	7.471	24.33	0.58	21.26				23.5919
Total		100.00		100.00				

(c)

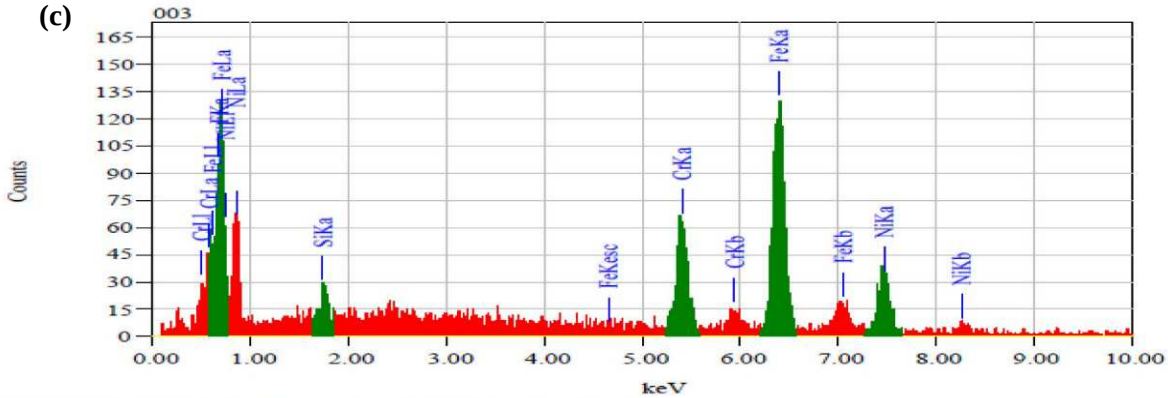

ZAF Method Standardless Quantitative Analysis
Fitting Coefficient : 0.2892

Element	(keV)	Mass%	Error%	Atom%	Compound	Mass%	Cation	K
F K*	0.677	2.56	0.05	7.09				4.6218
Si K	1.739	1.39	0.06	2.61				0.9521
Cr K	5.411	14.13	0.17	14.30				15.0380
Fe K	6.398	55.38	0.25	52.20				54.4709
Ni K	7.471	26.54	0.46	23.79				24.9172
Total		100.00		100.00				

Figure 10. EDS Spectrums from the Specimen: (a) Weld Metal, (b) Heat Affected Zone, and (c) Base Metal

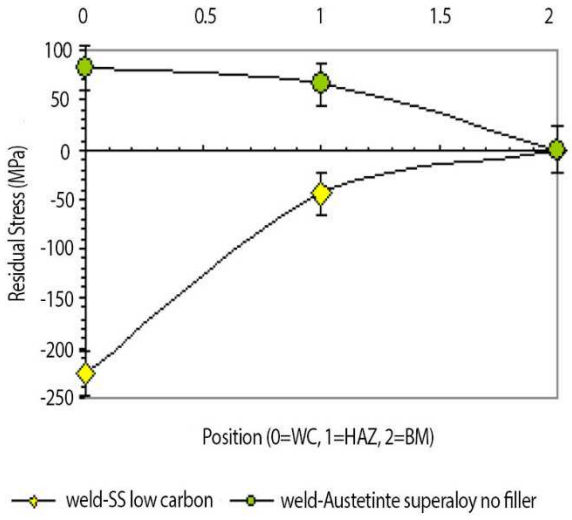

Figure 11. Comparison of the Residual Stresses Emerged from the Stainless Steel Specimens between SS-low Carbon with a Filler and Austenite Super Alloy 57Fe15Cr25Ni Welded No-filler

the welded plates employed in the offshore wind mono pile structures. The results have been discussed in terms of the role of welding sequence in damage inspections and structural integrity assessments of the offshore renewable energy structures. Furthermore, the reports have also been referred to in literature [5] and may be read to gain more insights of the residual stress phenomenon in welding materials.

4. Conclusions

Several techniques are available for the measurement of residual stress in the components of construction; however, measuring the effect of residual stress is not the stress of the rest. The non-destructive technique is to measure the magnitude of the relationship between stress and crystallographic nature (physics) in the component materials. Diffraction techniques as parts of non-destructive techniques measure the change in lattice spacing variation of polycrystalline material due to residual stress. With hydrostatic formulation, the amount of residual tensile stress in the specimen due to treatment of TIG welding without filler can be obtained from the magnitude of residual stresses serially from base metal, heat affected zone, and weld metal. They are 9.7 MPa, 92.1 MPa, and 75.62 MPa, respectively. This is confirmed by the microstructures observation, where carbon content might be very high in the dark lines. Weaken materials usually start from this side due to the presence of residual stress. This might initiate the inter-granular cracks, which are capable of migrating rapidly among the grain boundaries.

Acknowledgement

The writers would like to express their gratitude to the heads of PSTBM and BSBM, Dr. Azis Khan Jahja, Dr. rer. nat. Mohammad Dani, Drs. Bambang Sugeng, M.T., Rohmad Salam A.Md., and Agus Sujatno A.Md. for their kindness and helps. The writers would also like to thank DIPA 2015 for the financial supports.

References

[1] A.K. Jahja, N. Effendi, M.R. Muslich, J. Sci. Mater. Indones., 13/1 (2011) 34.
[2] N. Effendi, A.K. Jahja, Bandriana, W.A. Adi, Sci. J. Nucl. Fuel. Cycle. 18/1 (2012) 48.
[3] N.S. Rossini, M. Dassisti, K.Y. Benyounis, A.G. Olabi, Mater. Des., 35 (2012) 572.
[4] F. Hadjoui, M. Benachour, M. Benguediab, Mater. Sci. Appl., 3 (2012) 596.
[5] Parikin, Bandriyana, I. Wahyono, A.H. Ismoyo, Atom. Indones. J., 39/2 (2013) 65.
[6] T.K. Mandal, Mater. Sci. Poland., 33/1 (2015) 18.
[7] W. Wu, Z.W. Liu, J.J. Hua, Y. Zeng, Y.S. Li, J. Test. Eval., 40/3 (2012) 496.
[8] T.H. Priyanto, N. Effendi, Parikin, Adv. Mater. Res., 1123 (2015) 104.
[9] Parikin, T.H. Priyanto, A.H. Ismoyo, M. Dani, J. Mater. Sci. Indones., 17/1 (2015) 1-8 (in Indonesian).
[10] Parikin, N. Effendi, H. Mugihardjo, A.H. Ismoyo, J. Ilmiah. Daur. Bahan. Bakar. Nuklir., 20/1 (2014) 33 (in Indonesian).
[11] W. Zhang, J. Lu, K. Luo, Metals., 6/6 (2016) 1.
[12] A.K. Lisiecka, E.K. Ozgowicz, J. Ach. Mater. Manufact. Eng. JAMME, 44/2 (2011) 148.
[13] G.B. Marquis, Z. Barsoum, Procedia. Eng., 66 (2013) 98.
[14] H. Eisazadeh, J. Bunn, H.E. Coules, A. Achuthan, J. Goldak, D.K. Aidun, Welding Res., Welding J., 95 (2016) 111.
[15] S. Murugan, S.K. Rai, P.V. Kumar, T. Jayakumar, B. Raj, M.S.C. Bose, Int. J. Press. Vessels. Pip., 78 (2001) 307.
[16] A. Mehmanparast, O. Adedipe, F. Brennan, A. Chahardehi, Integrità. Strutturale., 35 (2016) 125. DOI: 10.3221/IGF-ESIS.35.15.